Proceedings of 23rd Annual Fellowship Symposium
Utah NASA Space Grant Consortium
May 8, 2017, Ogden, UT, USA

A NUMERICAL STUDY OF THE DEVELOPMENT OF INDUCER BACKFLOW

D. Tate Fanning *
Dept. of Mechanical Engineering
Brigham Young University
Provo, UT 84062
Email: tatefanning@byu.edu

ABSTRACT

Inducers are used as a first stage in pumps to hinder cavitation and promote stable flow. Inducers pressurize the working fluid sufficiently such that cavitation does not develop in the rest of the pump, which allows the pump to operate at lower inlet head conditions. Despite the distinct advantages of inducer use, an undesirable region of backflow and resulting cavitation can form near the tips of the inducer blades. This backflow is often attributed to tip leakage flow, or the flow induced by the pressure differential across an inducer blade at the tip. We examine backflow of a single inducer geometry at varying flow coefficients with a tip clearance of $\tau = 0.32\%$*, and no tip clearance. Removing the tip clearance prevents tip leakage flow. At all flow coefficients below design, we observe backflow penetrating up to* 14% *further upstream in the inducer with no tip clearance. The backflow region in the inducer with no tip clearance experiences higher velocities and extends further into the core flow. However, the inducer with tip clearance develops a larger vortex at the leading edge of the blades. A comprehensive analysis of these simulations suggests that diffusion as the working fluid is loaded onto the blades, not tip leakage flow, is the driving force for the formation of backflow.*

NOMENCLATURE

AR Area Ratio, $\frac{sin\beta_b}{sin\beta}$
C_m Meridional Velocity
C_p Pressure Recovery
D_{tip} Inducer Tip Diameter
i Incidence Angle
$\dot{m}_{back}$ Backflow Mass Flow
$\dot{m}_{in}$ Inlet Mass Flow
P Static Pressure
P_{inlet} Inlet Static Pressure
z Upstream Position
β Inlet Flow Angle
β_b Inlet Blade Angle
ϕ Flow Coefficient, $\dot{m}_{inlet}/(\rho A_{LE} U_{tip})$
ψ Head Coefficient, $(P_{outlet} - P_{inlet})/(\rho U_{tip}^2)$
τ Tip Clearance Ratio, $(Tip\ Clearance)/(D_{tip})$
U_{tip} Inducer Blade Tip Speed
ρ Density
σ Cavitation Number, $(P_{inlet} - P_{vapor})/(0.5\rho U_{tip}^2)$
Γ Circulation
V Velocity
ω Vorticity, $\nabla \times V$
η_a Diffuser Effectiveness

INTRODUCTION

An inducer is an axial rotor that imparts high pressures and velocities to the working fluid and is often placed immediately upstream of an impeller. The purpose of an inducer is to improve pump suction performance and widen the operating range, but inducers also introduce secondary flows. The most important secondary flow pertaining to an

*Address all correspondence to this author.

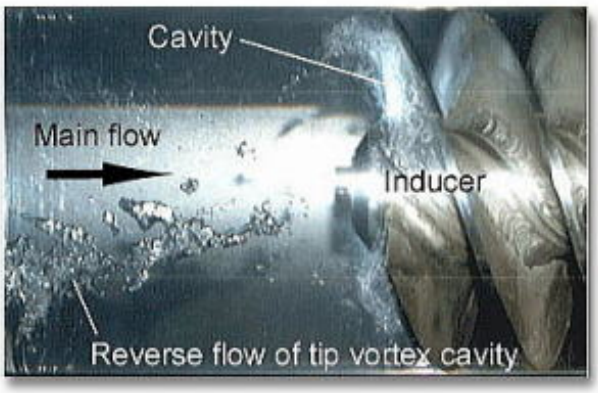

FIGURE 1. INDUCER UNDER CAVITATING CONDITIONS. CAVITY VOLUMES FOLLOW THE INDUCER BLADE TIPS AND PROPAGATE UPSTREAM DUE TO BACKFLOW.

inducer is backflow [1], which is a region of flow with a velocity component opposing that of the core flow.

Backflow is closely related to incidence, defined in Equation 1, where β_b is the inlet blade angle measured from tangential and β is the inlet flow angle measured from tangential. Backflow generally occurs at high incidence [1]. Significant backflow at the inducer leading edge causes unstable pump conditions [2, 3], which affects the incidence and overall pump performance [1]. Unstable incidence affects the rate of cavitation production and growth [4], which can lead to cavitation instabilities such as rotating cavitation or cavitation surge. Backflow that penetrates far upstream of the inducer restricts flow area, accelerating the inlet flow. This can lead to upstream cavitation, which grows and collapses with time [5]. Cavitation can further exasperate flow instabilities and cause reduced performance, or total pump failure. Figure 1 depicts a cavity following the tips of the inducer blades and propagating upstream due to backflow. The dynamics of backflow are responsible for cavitation instabilities [6].

$$i = \beta_b - \beta \tag{1}$$

Japikse's two-elements-in-series (TEIS) model is a useful way to better understand the inlet flow of an inducer [7]. TEIS is a 1D model where the inducer inlet from upstream to the throat is modelled as a diffuser. The area

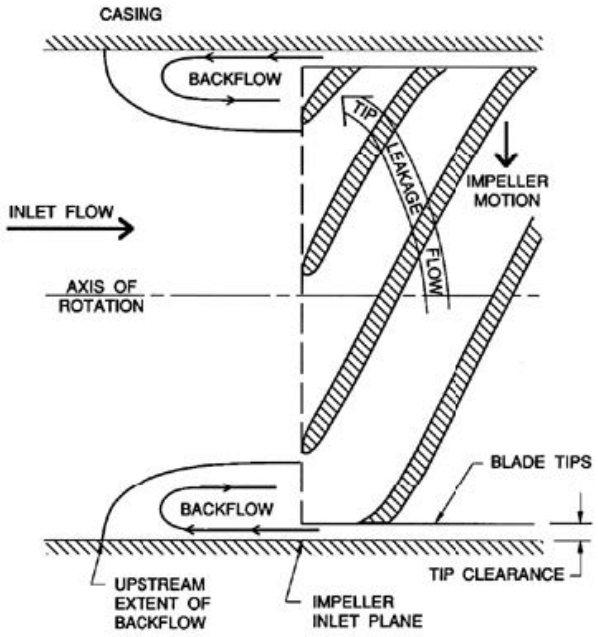

FIGURE 2. LATERAL VIEW OF IMPELLER ILLUSTRATING TIP LEAKAGE FLOW AND FORMATION OF THE BACKFLOW TIP VORTEX. ADAPTED FROM [1].

ratio (AR) of this diffuser is found using Eq. 2.

$$AR = \frac{sin\beta_b}{sin\beta} \tag{2}$$

As the incidence increases, the area ratio, and therefore diffusion will increase until a critical value is reached and the inducer stalls; which is the mechanism for backflow [8]. Japikse showed that at a critical area ratio, AR_{crit}, above ~ 1.5 the inlet will start to stall with resulting backflow [9, 10]. The ideal pressure recovery of this inlet diffusing section can be found from $1 - \frac{1}{AR^2}$. As the area ratio increases the pressure recovery, defined in Eq. 3, exceeds a critical value and the diffuser will stall [10]. This model provides the minimum approximate AR for backflow to occur. Inducers often operate close to this stall limit, because the high pressure recovery minimizes the growth of the vapor cavity and delays head breakdown [8].

$$C_p = \frac{P - P_{inlet}}{0.5\rho U_{tip}^2} \tag{3}$$

Prior studies, both experimental and numerical, have explored the cause and behavior of backflow. Experimental work has shown that inlet reverse flow can occur near the casing wall due to a significant axial pressure gradient adjacent to the inlet pressure surface between the blades because of the angle of attack of the blade, which causes the pressure rise to be produced in the first half of the inducer while leaving the latter half largely unloaded [11]. An axial momentum defect near the casing wall at the impeller inlet caused by the boundary layer also contributes to backflow formation [11], and is affected by tip clearance flow [12].

Computational studies have also explored the effect of tip clearance on backflow. Kim found that backflow penetrates further upstream and performance declines rapidly for larger tip clearances. For small tip clearances, upstream propagation is reduced, but flow begins to separate at the hub in the middle of the passage, also reducing performance [13]. You et. al. showed that larger tip clearance creates a larger tip vortex and creates negative pressure regions along the tip vortex in a linear cascade [14].

These studies attribute backflow to tip leakage flow, driven by the axial pressure gradient across the blade tip. Figure 2, adapted from [1] better illustrates how the pressure gradient between the pressure and suction sides of the blade causes flow to reverse direction and move back over the blade between the blade tips and pump casing. This flow generates a vortex structure near the leading edge of the blade [1] called the tip vortex. At flow coefficients below design, the blades are more heavily loaded, causing a more pronounced tip leakage flow [13].

The literature is mixed as to the precise cause of backflow and the role that incidence and tip leakage flow play. It is important to understand the precise cause of backflow to allow for inducer designs that improve performance and stability by minimizing backflow. In this work, we investigate the cause of backflow by comparing the characteristics of the generated backflow for both an inducer with tip clearance (TC) that allows tip leakage flow and an inducer with no tip clearance (NTC) to prevent tip leakage flow. Thus, the effects of inlet diffusion on backflow are assessed independent of tip leakage flow, allowing the cause of backflow to be isolated.

METHODS

A four blade inducer with a tip blade angle of 7° and a design flow coefficient of $\phi = 0.07$ is the subject of numerical simulations. This base geometry has a tip clearance of $\tau = 0.32\%$. The second inducer considered in this study is identical to the base geometry, however, the shroud radial position is reduced to be the same as the blade tip, resulting in zero tip clearance. The two modeled geometries are shown in Fig. 3. The commercial CFD package Star-CCM+ version 10.02.010 is used to test each inducer geometry over a range of flow coefficients ($\phi = 0.028, 0.042, 0.056, 0.07, 0.075$ and 0.08). The steady Reynolds-averaged Navier-Stokes equations are solved with a 2nd-order upwind convection scheme and segregated solver. The realizable K-ε model, which uses wall functions for regions of the mesh with high y^+ values and assumes the viscous sublayer is properly resolved for regions with low y^+ values is used to model turbulence [15].

The inducer computational domains were defined by meshes generated in Star-CCM+. The meshes have $5.6 * 10^6$ and $6.0 * 10^6$ polyhedral cells for the NTC and TC inducers, respectively, with refinement near the inducer blades and hub, as seen in Fig. 3, to better capture the tip vortex. The average y^+ value for the mesh was 8. Lundgreen performed grid independence studies using the same TC inducer geometry and found that machine performance monitors such as inducer head coefficient varied by less than 0.35% when the mesh size was increased to $12.2 * 10^6$ cells from $6.5 * 10^6$ [5]. Therefore, for this work, the mesh sizes are considered sufficiently refined and error of critical monitors is assumed to be on the order of 0.5%. Convergence was determined case by case by evaluating the solution monitors of inlet mass flow, outlet mass flow, inlet total pressure, head coefficient, and rotordynamic forces of the inducer blades. NTC inducer simulations at the lowest flow coefficients tested ($\phi = 0.028, 0.042$) produced quasi-steady solutions. In these cases, the solutions were considered converged when the solution monitors exhibited the same periodic behavior over 10 blade revolutions. To confirm the validity of these low ϕ NTC simulations, additional unsteady simulations at $\phi = 0.028$ and $\phi = 0.042$ were performed with a time step of 0.001 s. The steady simulation monitors were found to deviate from the unsteady values by less than 1%.

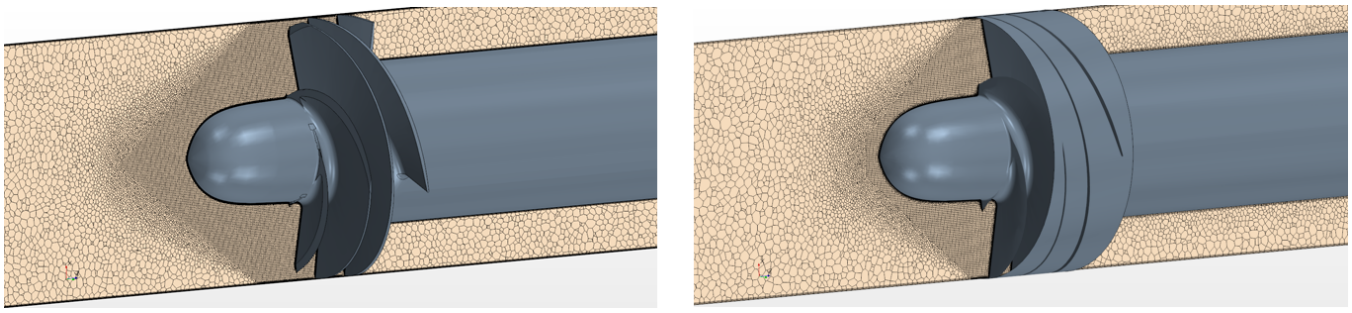

FIGURE 3. CONSIDERED INDUCER GEOMETRIES AND CORRESPONDING MESHES. THE BASE INDUCER GEOMETRY IS ON THE LEFT AND THE GEOMETRY WITH NO TIP CLEARANCE IS ON THE RIGHT.

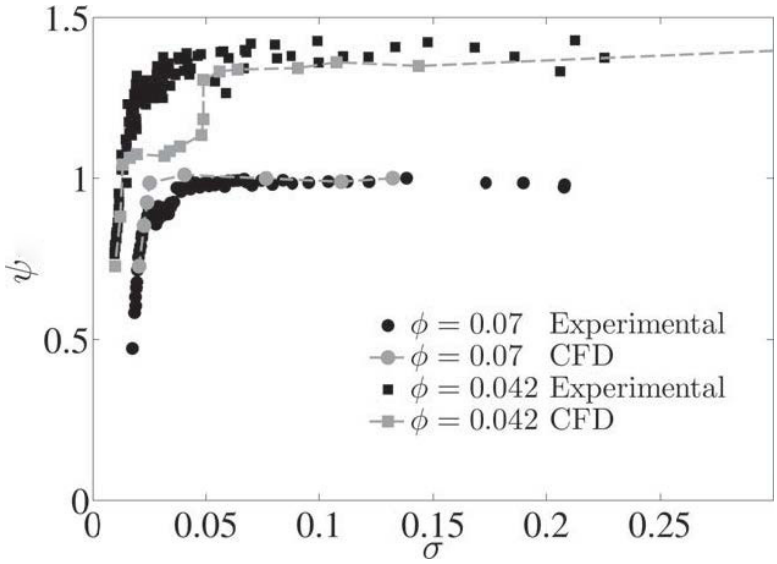

FIGURE 4. BREAKDOWN CURVE OF AN INDUCER WITH AN INLET BLADE ANGLE OF 7°. THE BREAKDOWN CURVES PRODUCED BY CFD PRODUCE RESULTS VERY COMPARABLE TO THE EXPERIMENTAL RESULTS AND VALIDATE THE FLOW PHYSICS MODELING.

RESULTS

Various measures to characterize the backflow are explored. Analysis using AR instead of ϕ is perhaps the most useful because AR accounts for both blade angle and flow coefficient. AR therefore describes more directly both incidence and inlet diffusion. Figures 5 and 6 show the relationship between AR and backflow penetration and mass flow, respectively. Figure 5 shows backflow penetrates $\sim 0.1D_{tip}$ at $AR = 1.5$. As AR increases, backflow penetration also increases to a maximum of $5.4D_{tip}$ and $4.6D_{tip}$ at $AR = 4.3$ for the NTC and TC cases, respectively. Recall that Japikse posited a critical area ratio where backflow would occur at a value of $AR_{crit} = 1.5$. This predicted limit closely matches the CFD results. Figure 6 shows the backflow mass flow at the leading edge. There is minimal mass flow at AR_{crit}, but above AR_{crit}, mass flow increases almost linearly with increasing AR. Both plots suggest a strong relationship between AR and the backflow vortex. As the area ratio increases, diffusion increases as a result, until a critical value is reached and the inducer stalls, which is the primary mechanism for backflow [8]. Note that the backflow mass flow at low AR is higher in the TC inducer due to the tip leakage. This tip leakage flow causes the recirculation mass flow to be higher for the TC case, but appears to not have any effect on the axial extent of the backflow vortex, suggesting that backflow penetration is a result of inlet diffusion, not tip leakage flow.

Figures 7, 8, and 9 provide more insight into back-

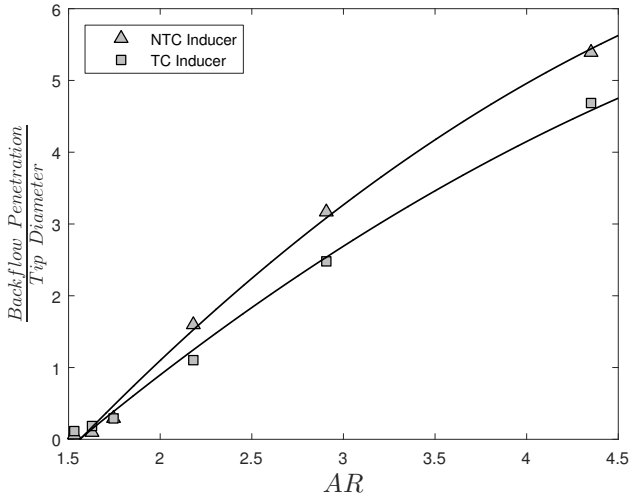

FIGURE 5. NON-DIMENSIONAL BACKFLOW PENETRATION AS A FUNCTION OF *AR* FOR ALL TESTED FLOW COEFFICIENTS. POLYNOMIAL CURVE FITS FOR EACH DATA SET ARE SHOWN. THE CORRELATION WITH AREA RATIO FURTHER SUGGESTS INLET DIFFUSION AS THE MAIN FORCE DRIVING BACKFLOW.

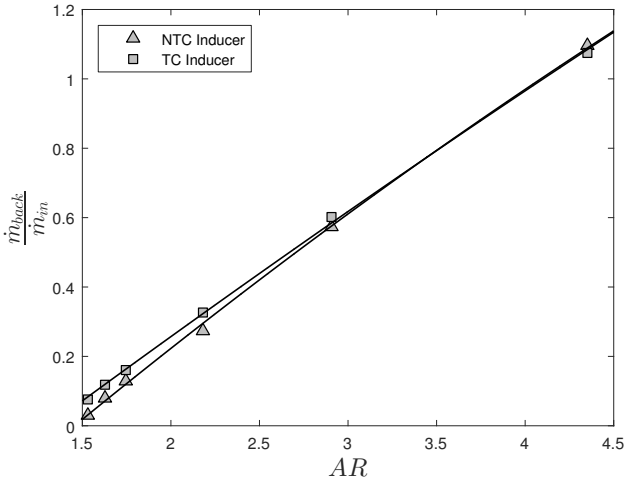

FIGURE 6. NON-DIMENSIONAL BACKFLOW MASS FLOW AS A FUNCTION OF *AR* FOR ALL TESTED FLOW COEFFICIENTS. POLYNOMIAL CURVE FITS FOR EACH DATA SET ARE SHOWN. THIS STRONG RELATIONSHIP FURTHER SUGGESTS INLET DIFFUSION AS THE MAIN FORCE DRIVING BACKFLOW.

flow differences and show non-dimensional axial velocity through the span of the blades for $AR = 4.35$ and $AR = 1.53$ at positions upstream of the leading edge where $\frac{z}{D_{tip}} = 0.5,\ 1.5$, and 3, respectively. These plots show minor variation between fluid velocity profiles at the higher flow coefficient because backflow is restricted to the relatively small tip vortex. However, at high *AR*, significant backflow is present, with variation in velocity and percent span where backflow occurs between NTC and TC geometries. At $\frac{z}{D_{tip}} = 0.5, 1.5$ and 3, backflow velocity near the casing wall is greater (45.9%, 63.8%, and 69.8% respectively) in the NTC inducer. However, the region of backflow occurs at a lower span for the TC inducer for $\frac{z}{D_{tip}} = 0.5$ and 1.5, but not for $\frac{z}{D_{tip}} = 3$. Analysis of span where flow reverses helps describe the shape of the backflow; namely that is not constant with upstream position. Near the leading edge of the blades ($\frac{z}{D_{tip}} = 0.5$) for $AR = 4.35$ in the NTC inducer, backflow thickness is $\sim 15\%$ of span. However, at $\frac{z}{D_{tip}} = 1.5$, backflow occupies $\sim 20\%$ of the span, and increases to almost 40% of the span at $\frac{z}{D_{tip}} = 3$. For the TC inducer at $AR = 4.35$, backflow thickness is $\sim 20\%$ of span at ($\frac{z}{D_{tip}} = 0.5$), and increases to $\sim 25\%$ at both $\frac{z}{D_{tip}} = 1.5$ and 3. In both geometries, backflow thickness increases with increasing upstream position, up to a maximum. Past this point of maximum thickness, thickness decreases with further increasing upstream position until backflow terminates. The distance between the point of maximum backflow thickness and the leading edge increases with increasing *AR*. The backflow thickness is small near the inducer tip likely because of the influence of the nose cone that accelerates the flow as fluid enters the blades.

Figures 10 and 11 show two distinct vortices: a small tip vortex that is caused by the interaction of the casing boundary layer and the leading edge of the blade, and a larger backflow vortex due to inlet stall. These figures depict the tip vortex turbulent kinetic energy and streamlines colored with vortex magnitude for the NTC and TC inducers operating at $AR = 2.9$, respectively. Showing the scalar values of turbulent kinetic energy along with streamlines provides an empirical method of determining vortex size and strength. From these images, it is clear the TC inducer exhibits a larger, more powerful tip vortex. Figure 12 provides a more quantitative comparison of vortex strength. In this figure, only the strength of the tip vortex is considered, and is compared to *AR*. Circulation (Γ) is defined in Equation 4 and is the amount of swirl in a vortex. Circulation was determined by first defining a closed plane region at

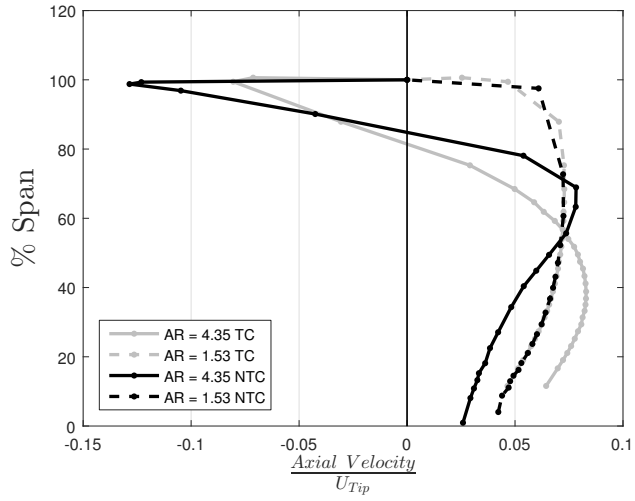

FIGURE 7. PLOT OF NON-DIMENSIONAL AXIAL VELOCITY THROUGH THE BLADE SPAN FOR AN AXIAL LOCATION OF $\frac{z}{D_{tip}} = 0.5$.

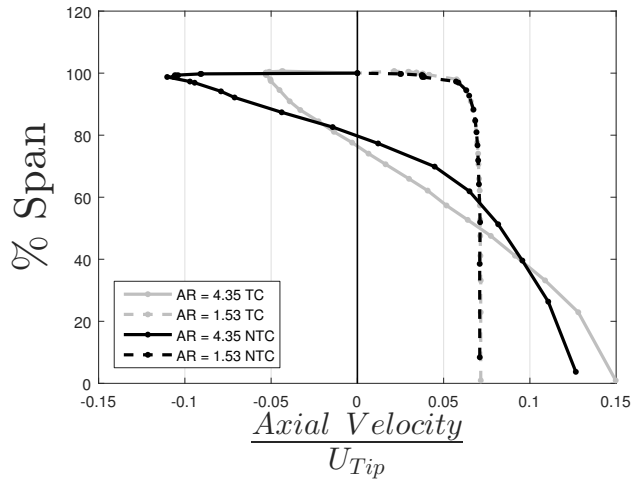

FIGURE 8. PLOT OF NON-DIMENSIONAL AXIAL VELOCITY THROUGH THE BLADE SPAN FOR AN AXIAL LOCATION OF $\frac{z}{D_{tip}} = 1.5$.

the leading edge of a single blade encompassing the full tip vortex. This region was constant through the range of tested AR, and was sufficiently large to capture the full volume of the largest vortex. At all tested AR, the tip vortex of the TC inducer was determined to have $23.7\% - 40.8\%$ greater circulation. That is to say, the TC inducer has a more powerful tip vortex at all tested AR. It is clear that tip leakage flow increases with increasing AR and significantly

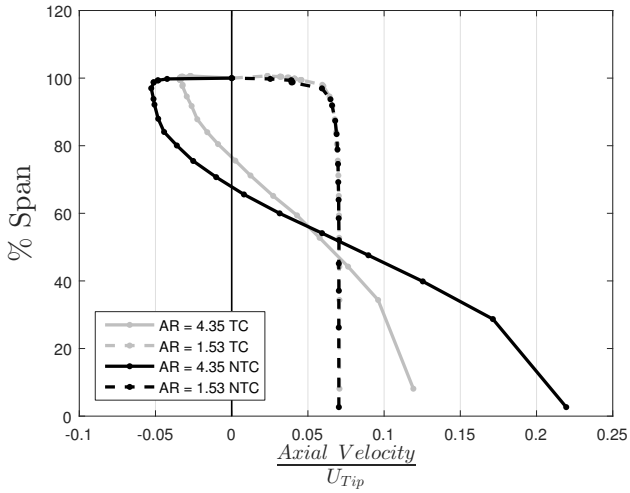

FIGURE 9. PLOT OF NON-DIMENSIONAL AXIAL VELOCITY THROUGH THE BLADE SPAN FOR AN AXIAL LOCATION OF $\frac{z}{D_{tip}} = 3$.

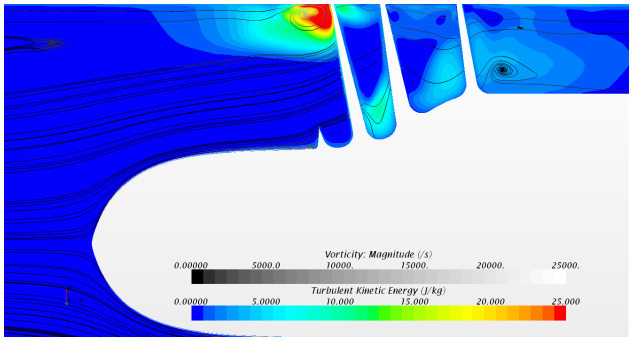

FIGURE 10. NTC INDUCER OPERATING AT $AR = 2.9$.

increases the tip vortex size and strength. Tip leakage contributes to the strength of the tip vortex, but it is not the root cause. Likewise, the tip leakage does not cause backflow, nor does it appear to even contribute to it.

$$\Gamma = \oint_{\partial S} V \cdot dl = \int\int_{S} \boldsymbol{\omega} \cdot dS \tag{4}$$

To better understand the cause of backflow, we turn to the TEIS model, which looks at the inlet of the inducer as a diffuser. Figure 13 shows C_p, calculated using Eq. 3 and CFD predictions of static pressure along the casing, at various axial positions for $AR = 1.75$. The solid vertical line corresponds to the blade leading edge location. The maxi-

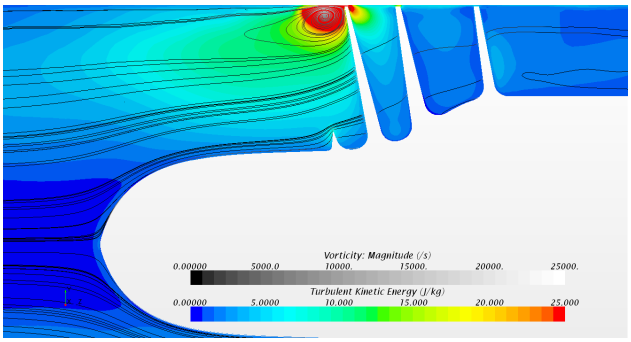

FIGURE 11. TC INDUCER OPERATING AT $AR = 2.9$.

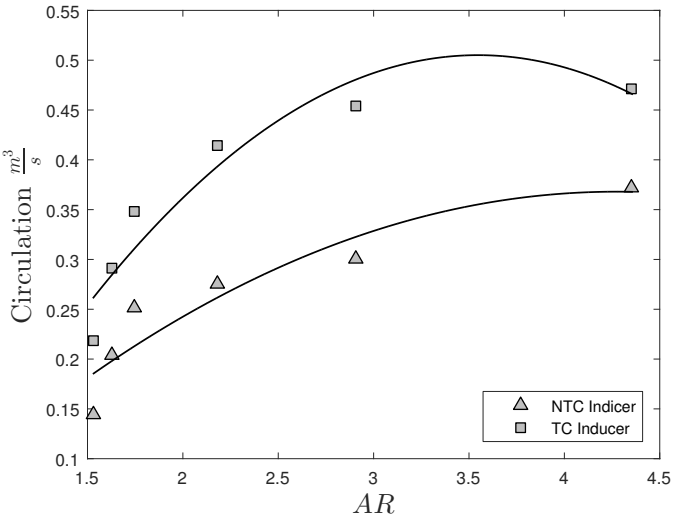

FIGURE 12. TIP VORTEX CIRCULATION AS A FUNCTION OF AREA RATIO. AT ALL TESTED *AR*, THE TC INDUCER TIP VORTEX HAS A GREATER CIRCULATION, SIGNIFYING THE TIP VORTEX IS STRONGER IN THE TC INDUCER CASES.

mum value of C_p occurs slightly downstream of the leading edge. Figure 14 shows that maximum pressure recovery increases with increasing *AR*. In all cases, the NTC inducer exhibits a greater pressure recovery across the range of flow coefficients, which is consistent with the greater backflow already discussed. The pressure recovery is higher for the NTC case because there is no tip clearance, which loads the blade tip and increases the achievable pressure rise.

CONCLUSIONS

This work explored the effects of tip clearance, tip leakage flow, and inlet flow area ratio on the inlet flow field of

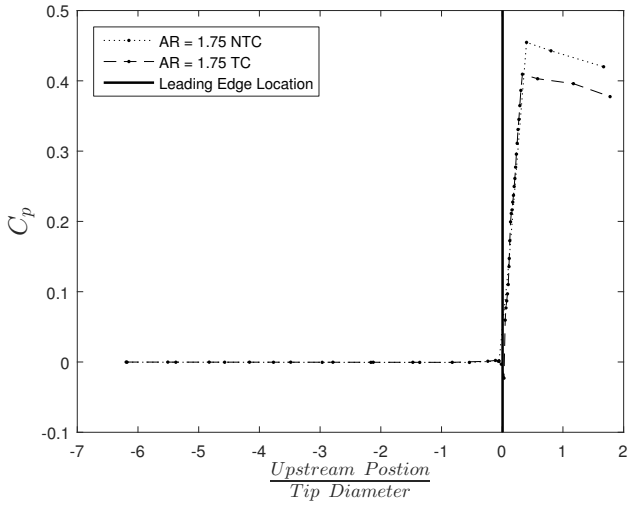

FIGURE 13. PRESSURE RECOVERY OVER A RANGE OF AXIAL POSITIONS FOR A SINGLE *AR*. THE SOLID VERTICAL LINE REPRESENTS THE LOCATION OF THE LEADING EDGE OF THE INDUCER BLADES. THE NTC INDUCER EXPERIENCES GREATER PRESSURES DOWNSTREAM OF THE LEADING EDGE, SIGNIFYING GREATER INLET DIFFUSION THAN IN THE TC INDUCER.

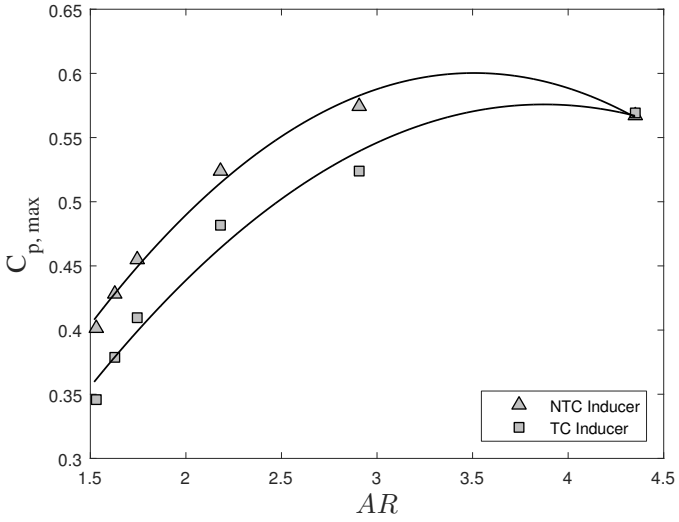

FIGURE 14. PRESSURE RECOVERY AS A FUNCTION OF AREA RATIO. THE NTC INDUCER EXPERIENCES A GREATER PRESSURE RECOVERY, SIGNIFYING GREATER FLUID PRESSURES IN THE INDUCER INLET. THE GREATER FLUID PRESSURES CORRESPOND TO LOW FLUID VELOCITIES AND A HIGH INLET DIFFUSION.

an inducer. In cases where backflow is present there are two vortex structures upstream of the leading edge: a small tip vortex and a larger backflow region. Removing the inducer tip clearance to prevent tip leakage flow was shown to increase backflow over the case with tip clearance and leakage flow. The main driving force behind inducer backflow therefore cannot be tip leakage flow. The tip leakage flow contributes to the strength of the tip vortex that is produced by the interaction of the casing boundary layer with the leading edge of the inducer. This tip vortex is often confused with backflow in literature. The greater tip leakage flow at higher area ratios generates a larger tip vortex, but has marginal if any effect on backflow. The pressure recovery at the inducer inlet along the casing is greater at all flow coefficients for the NTC inducer. Comparing backflow penetration and mass flow to inducer inlet area ratio produces a strong relationship and indicates that the primary mechanism for backflow is high inducer inlet diffusion due to the high incidence at the leading edge. Current understanding of backflow has limited the design space of high performance pump inducers. By understanding that inlet diffusion is the main factor influencing backflow, designers can focus more on limiting diffusion and stall events at the inducer inlet to produce higher performing inducers.

ACKNOWLEDGMENT

This work received no specific grant from any funding agency in the public, commercial, or not-for-profit sectors.

REFERENCES

[1] Brennen, C., 1994. *Hydrodynamnics of Pumps*. Concepts ETI, Inc. and Oxford University Press.

[2] Tani, N., Yamanishi, N., and Tsujimoto, Y., 2012. "Influence of flow coefficient and flow structure on rotational cavitation in inducer". *Journal of Fluids Engineering,* ***134***.

[3] Makay, E., 1980. "Centrifugal pump hydraulic instability". *Electric Power Res. Inst. Rep. DPRI CS-1445*.

[4] Vlaming, D., 1989. "Optimum impeller inlet geometry for minimum npsh requirements for centrifugal pumps". *Pumping Machinery ASME FED-81*, pp. 25–29.

[5] Lundgreen, R., 2015. "Improving the suction performance and stability of an inducer with an integrated inlet cover bleed system known as a stability control device". PhD thesis, Brigham Young University.

[6] Badowski, H., 1969. "An explanation for instability in cavitating inducers". *ASME Cavitation Forum*, pp. 38–40.

[7] Japikse, D., Marscher, W., and Furst, R., 1997. *Centrifugal Pump Design and Performance*. Concepts ETI, Inc.

[8] Oliphant, K., Lundgreen, R., Cluff, R., Maynes, D., and Gorrell, S., 2013. "Inducer design for stable high suction performance, wide operating range, adn increased structural robustness utilizing a high mass flow gain inlet cover treatment". *Joint Army Navy NASA Air Force Converence*.

[9] Japikse, D., 1984. "A critical evaluation of stall concepts for centrifugal compressors and pumps - studies in component performance, part 7". *Stability, Stall, and Surge in Compressors and Pumps*, pp. 1–10.

[10] Qiu, X., Japikse, D., and Anderson, M., 2008. "A meanline model for impeller flow recirculation". *ASME Turbo Expo 2008: Power for Land, Sea, and Air, American Society of Mechanical Engineers*, pp. 1687–1694.

[11] Aoki, M., and Yamamoto, K., 1992. "Inlet reverse flow mechanism in axial flow turbomachines with neither stall nor significant radial flow". *Journal of Turbomachinery,* ***114***(2), pp. 392–397.

[12] Yokota, K., Kurahara, K., Kataoka, D., Tsujimoto, Y., and Acosta, A., 1999. "A study of backflow vortex structure at the inlet of an inducer". *ASME Journal of Fluids Engineering,* ***129, No. 3***, pp. 587–593.

[13] Kim, S., Choi, C., Kim, J., Park, J., and Baek, J., 2013. "Effects of tip clearance on performance and characteristics of backflow in a turbopump inducer". *J. Power and Energy,* ***227***(8), pp. 847–857.

[14] You, D., Wang, M., and et al., P. M., 2004. "Study of tip-clearance flow in turbomachines using large-eddy simulation". *Comput. Sci. Eng.,* ***6***, pp. 38–46.

[15] CD-Adapco, 2015. "Help files, star-ccm+ version 10.02".